A Study of Symmetry Breaking and Stability in Conical Shells and the Implications for Actuators

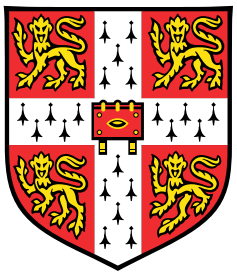

Arathi Ramachandran

Department of Materials Science & Metallurgy
University of Cambridge

This dissertation is submitted for the degree of
Doctor of Philosophy

Sidney Sussex College August 2017

In loving memory of my beloved grandfather, N.R. Krishnaswamy

Declaration

This dissertation is the result of my own work and includes nothing which is the outcome of work done in collaboration except as precisely indicated in the text. My research was conducted under the supervision of Dr. J.A. Elliott between March 2015 and December 2016 and Dr. Stoyan K. Smoukov between September 2012 and March 2015 in the Department of Materials Science & Metallurgy of the University of Cambridge. No part of this dissertation has been submitted for consideration for any other degree at this or any other university. Some of the material presented in Chapter 3 was presented as a talk at the Spring Materials Research Society(NN). In accordance with the requirements of the Degree Committee of the Faculty of Physics and Chemistry, this dissertation, excluding references, does not exceed 60,000 words.

Arathi Ramachandran
August 2017

Acknowledgements

The beautiful thing about this PhD is at has been a continual unfolding of problems both on a personal and technical level, so I have yet a whole new set of people to thank in addition to the pre-correction set- so I hope the committee does not mind me adding to my previous list since I anyway was asked to revise and restructure the thesis- it does seem like this may have been part of my PhD! I am grateful to the new Krishna who has entered my life and given me joy!!! He has introduced me to a number of people who have helped me, discussed with me, and given me additional support I needed to finish: namely Jai Prakash Navanedhakrishnan(thank you for helping me to format my thesis so it looked better) and Vivek Dabade(thank you for asking me the question of what are the minimal parameters to describe the shell as this question helped me to frame the literature in a way where I could think). I am also thankful to Naveen Chandiran for his help.Thank you to Umesh Ji who gave me the personal guidance I needed to deal with my fears. I am exceedingly grateful to my parents who have truly showed me unconditional love this past year. I am incredibly lucky to have such gentle and supportive parents. I have very literally put them through hell and back this year. I am very grateful to my committee namely for wording my corrections in a thoughtful way that allowed me to more gently address the deeper issues that I needed to think about further, this enabled me to confront my own fears and tap into the curiosity I do have despite my background. I learnt alot while addressing my corrections. I am grateful to James Elliott, Rosie Ward, Ruth Cameron for having faith in me and helping me transition and keep going.Thank you to Keith Seffen for helping me to find the curiosity I do have, not judging me, and helping me anywayt. I can finally understand why you were stimulating me to think about the cap/cone interaction. I feel grateful that J.F. Scott talked with me about my problem, when I felt like I had nothing to say technically- that in itself meant alot to me. I am grateful to James Dean for helping me learn ABAQUS. I am grateful to Rachel Kurchin, CJ Luo, and Giovanni Offedu who made my first year just bareable. In my own way I am grateful to Stoyan Smoukov for the questions I never would have had the audacity to approach otherwise and introducing me to ideas that I had never thought about. Not only do I have one set of really loving parents, but I am lucky to have Raja mama and Prabha mami as my aunt and uncle - they are another set of parents! I am grateful to my grandmother, Usha

Patti, for her loving strength and steely support. I have three exceedingly loyal and beautiful friends: Gabi, Anya, and Nimrod who also loved me unconditionally when I was at my worst. My friends from pika Anya, Nimrod, Alorah, Galina, and Aga could always be counted upon to provide adventure! Anya, Nimrod, and Alorah sent me mysterious packages for a year just to cheer me up!! I am lucky to have a long list of mentors and teachers on whom I can always rely on! These include Professor Alison Malcolm, Professor Lorna Gibson, Professor Jeffrey Grossman, Professor Hobbs, Professor Alexie Kolpak, Dr. Chang-Jun Bae, Mrs. Yaffie, and Mrs. Spradley. My Sidney home, pika home- a massive list of friends (Rachel Mc Callister, Joana, Katie, Yssy, Maitreyi, Jan, Mansur, Sarwat, Xiao, Gregory, Wei Li, Galina) made this journey meaningful in so many ways.

Abstract

This thesis primarily explores the stability of spherically capped conical shells and secondarily explores the nature of the polygonal folds observed during these deformations. The polygonal folds were classified according to the number of facets observed. The problem is primarily explored using Finite Element Method (FEM) studies of rigid indentations of spherically capped conical shells of varying thickness, cone angle, and slant height. The main finding of the FEM studies is that the capped shells suddenly buckle during the indentation as the ridge approaches the region where the cap and conical shell meet. The geometry of this join region dominates the shell response for all the studied spherically capped conical shells and provides another perspective on how local geometry affects a shell's response to indentation. Experimentally a commercially bought rubber conical shell is qualitatively observed to show that the shell can be poked and folded to remain statically in a wide number of folded shapes. While the thesis does not answer the reason for this stability, the combination of the FEM studies and exploration of the rubber conical shell suggest that the observed stability is likely linked to the interaction between the cap and conical shell.

List of symbols and variables

Table 1 All Variables and Symbols

Variable name	symbol	units
Engineering strains	ε_i	
Principal stretches	λ_i	
Stress	σ_{ii}	MPa
radial coordinate	ρ	
Young's modulus	E	MPa
Bulk modulus	B	MPa
Shear modulus	G	MPa
Poisson ratio	ν	
Strain energy function	W	$\frac{J}{mm^3}$
Neo-Hookean constant	C_{10}	GPa
Neo-Hookean constant	D_1	GPa^{-1}
Spherical cap radius	r	mm
Spherical cap height	h	mm
Shell thickness	t	mm
Cap base radius	l_{sp}	mm
Half cap solid angle	β	rad
Base radius	R	mm
Cone angle	α	mm
Cone slant height	l	mm
Indenter radius	r_i	mm
Bending stiffness	D_B	mJ
Stretching stiffness	D_S	MPa mm
Critical shell thickness	t_c	
Shallow spherical shell param	Λ	
Deep spherical shell param	Λ_d	
Axial compression load coefficient	C	
Total axial load at diamond pattern buckling	P	N
Deflection in cartesian coordinates	$w(\rho)$	
Airy stress function	ψ	
Delta function	$\delta(\rho)$	
Displacement	δ	mm
Force	F	N
Indenter radius	r_i	mm
Indenter shell geometry	γ	
Distance from tip of initiated fold	δ_{start}	mm
Displacement of downward load	δ_{down}	mm
Displacement of load removal	δ_{lift}	mm
Spherical shell control parameter	$\Delta = \frac{\delta}{t}$	
Cap cone join parameter	$\delta_j = \frac{\delta}{h}$	
Spherical ridge parameter	$\delta_{ridge} = \frac{\delta}{\sqrt{rt}}$	
Indenter shell geometry	$\gamma = \frac{r_i}{r}$	
Spherical shell ridge	$r_{ridge} = \sqrt{r\delta}$	
Spherically capped conical shell parameter	$\delta_{capcone}$	

Table of contents

List of figures

List of tables

Chapter 1

Introduction

1.1 Multistability, shells and applications

My thesis problem began with the simple observation that a silicone rubber cone that I had purchased appeared to have a number of 'metastable' states. When poking the silicone shell with a pen at its tip, or simply folding over an edge of the shell, the shell remained static in the deformed shape for extended periods of time (over a month) without any obvious change in shape. The deformed shell also showed polygonal folds that have been observed in indentation of zero and positive Gaussian curvature shells[25]. I sought to understand why I observed these metastable states and if these metastable states might have some applications for a soft robotic actuator, and understand the effect of the conical geometry on the observed deformation.

1.2 Stability and thin shells

For thin shells the competition between in-plane stretching and out-of plane bending energies is what results in the complexity of their behavior as well as the existence of stable, deformed states. Both geometry and materials properties determine how energy is stored in the deformed shell structures. Both thin shallow conical frustum and shallow spherical caps made of homogeneous materials are known to have bistability, or two stable states for a wide variety of initial parameters[25].

1.2.1 Materials properties and stability

Most continuum models of materials are based on modeling the behavior of materials on ideal springs. Ideal springs respond proportionately to an applied force and do not dissipate

energy when stressed. Real materials behave in more complex ways than a simple spring. If it were possible to make a shell from connecting an infinite number of perfect, elastic, Hookean springs, the deformation of this object would only be determined by the geometry. In real materials, 1) extension in different directions are coupled(i.e. Poisson effect), 2) the material stress response may be direction dependent(i.e. anisotropy), 3)responses are non-linear for certain strains, and 4) energy may be dissipated(i.e materials can have non-elastic behavior). Materials can deform permanently or show more complex time dependent behavior.

Poisson effect

As mentioned, unlike a perfect spring when a strip of some physical material is subjected to a force in one direction it deforms, generally contracts, in the two perpendicular directions as well as deforming in the direction of the applied stress, this is known as the Poisson effect. The Poisson ratio,ν, is a measure of the perpendicular contraction of the material. For an isotropic material the following equation, Eq.1.1, describes the relationship between deformations of the material in different directions.

$$\nu = -\frac{d\varepsilon_y}{d\varepsilon_x} = -\frac{d\varepsilon_z}{d\varepsilon_x}. \tag{1.1}$$

Generally ν varies between 0 and 0.5(investigation of auxetic materials or materials with a Poisson ratio less than 0 is an ongoing field of investigation [24]). As ν approaches 0.5, the material behaves closer to an incompressible material. No solid is truly incompressible, many liquids can be treated as incompressible(i.e. volume is conserved). Rubbers and some polymers, however, are unusual in that they do have Poisson ratios close to 0.5, when deformed at low frequencies[15]. At higher frequencies or when the polymer is near its glass transition most polymers have lower Poisson ratios (~ 0.3) [15].The bulk modulus, B, which is a direct measure of how compressible a material is related to ν by

$$B = G\frac{2(1+\nu)}{3(1-2\nu)}, \tag{1.2}$$

where G is the shear modulus. As shown in this expression as ν approaches 1/2, $\frac{B}{G}$ diverge, however in practice when the bulk modulus is measured for many of these polymeric materials little to no change is observed [11]. With respect to the problem of stable states of deformed shells, these materials properties such as the Poisson ratio affect how energy is stored in the deformed shells (i.e. the observed stretching and bending of the shell) and therefore the stable states accessible to the shell. One way of understanding how these materials properties affect the behavior of the shell is by considering the effect they have on bending and stretching

stiffnesses. In a shell, only the bending stiffness, D_B, has a dependence on the Poisson ratio.

$$D_B = \frac{Et^3}{1-\nu^2} \tag{1.3}$$

Therefore as ν is increased the bending stiffness, D_B increases. As the bending stiffness is increased, fewer creases and folds are expected in the deformed shell. Both the bending and stretching stiffnesses,D_B and D_S respectively, depend on the material's Young's modulus and the shell's thickness.

$$D_S = Et \tag{1.4}$$

Madhukar et. al observe that by increasing the Poisson's ratio of the cap the energy stored in the cap is increased [10]. Sobota and Seffen's simulations also show that as the Poisson ratio is increased the critical initial midpoint deflection at which bistability is observed increases [18].

Anisotropy vs. Isotropy

While most materials such as common metals, common metal alloys, most rubbers, and so on are isotropic(i.e their response is not orientation dependent), materials such as composites, highly oriented polymeric materials, anisotropic crystalline materials among other materials respond differently when stressed along different directions. Shells made of anisotropic materials will deform to store energy along certain preferred directions in the material. These materials can be used to create bistable shells, where the same shape isotropic shell would not be bistable. For example, cylindrical shells and tapes made from anisotropic materials such as fiber reinforced composites are bistable due to the behavior of the composite materials in addition to the shell geometry [7].

Nonlinear materials behavior

Many common materials respond linear elastically for small strains and deform plastically(i.e. non-elastic and nonlinear behavior) for larger strains. Some notable materials like rubbers and biological tissues show an elastic nonlinear response for large strains. These materials including the rubber from which the snow cones that sparked this thesis are made need to be characterized by a full stress-strain curve.

History dependent materials behavior

Materials can also have history dependent behavior. Any kind of flow or viscous behavior is a history dependent material. Many plastics show viscoelastic behavior, which means that

for typical strains under certain frequencies, the material flows like a liquid, but also exhibits solid like elastic behavior. When making a thick shell out of a viscoelastic material, the time dependent behavior of the material can be used to fabricate a pseudobistable cap that everts and remains static for a period of time and then snaps back to its original state[16].

Hyperelastic materials

Hyperelastic materials are materials that behave elastically for large strains. Hyperelastic materials are non-linear materials, i.e. their stress-strain curves are not linear over these large strains under which they deform elastically. These materials are defined in terms of an elastic potential function, W, which can be defined as a function of the strain tensor and stress tensor. It is often simpler to express W in terms of invariants I_1,I_2, I_3 , and J of these tensors which are given by

$$I_1 = (\lambda_1)^2 + (\lambda_2)^2 + (\lambda_3)^2 \tag{1.5}$$

$$I_2 = (\lambda_1)^2(\lambda_2)^2 + (\lambda_2)^2(\lambda_3)^2 + (\lambda_3)^2(\lambda_1)^2 \tag{1.6}$$

$$I_3 = (\lambda_3)^2(\lambda_2)^2(\lambda_3)^2 = J^2 \tag{1.7}$$

where λ_i are principal stretch ratios, which are related to engineering strain, ε_i, by

$$\varepsilon_i = (\lambda_i) - 1 \tag{1.8}$$

[17].

Since most rubbers are incompressible the simplification $I_3 = 1$ is usually applicable. The Mooney-Rivlin model is one of the simpler hyperelastic materials model and the Neo-Hookean model, which I use later in the thesis is a further simplification of the Mooney-Rivilin model. The Neo-Hookean model, is given by

$$W = C_{10}(\bar{I}_1 - 3) + \frac{1}{D_1}(J-1)^2 \tag{1.9}$$

.

where C_{10}, and D_1 are materials constants that deal with shear, and bulk compressibility respectively, and $\bar{I}_1 = J^{-1}I_1$ [17].

Both the Mooney-Rivlin and Neo-Hookean hyperelastic models do not capture the strain stiffening that hyperelastic materials exhibit for very large stretches [17]. If a hyperelastic material is treated as though it is incompressible and has a Poisson ratio of $\nu \approx 0.5$, then the following stress- strain relations are obtained.

$$\sigma_{11} - \sigma_{33} = 2((\lambda_1)^2 - (\lambda_3)^2)C_{10} \tag{1.10}$$

.

$$\sigma_{22} - \sigma_{33} = 2((\lambda_2)^2 - (\lambda_3)^2)C_{10} \tag{1.11}$$

.

The stress strain relation for an incompressible, Neo-Hookean material under uniaxial tension is

$$\sigma_{11} = 2C_{10}(\lambda^2 - \frac{1}{\lambda^2}) \tag{1.12}$$

.

1.2.2 Stability of spherical shells

Homogeneous spherical shells can be monostable, pseudobistable, and bistable. When a thin spherical shell that can only undergo shell extension or meridian compression is indented as shown in Fig. 1.1a, the force response of the shell is as shown in Fig. 1.2b [21]. As the thickness of the shell is increased the bending stiffness of the shell increases and the load profile changes as shown in Fig. 1.1c.

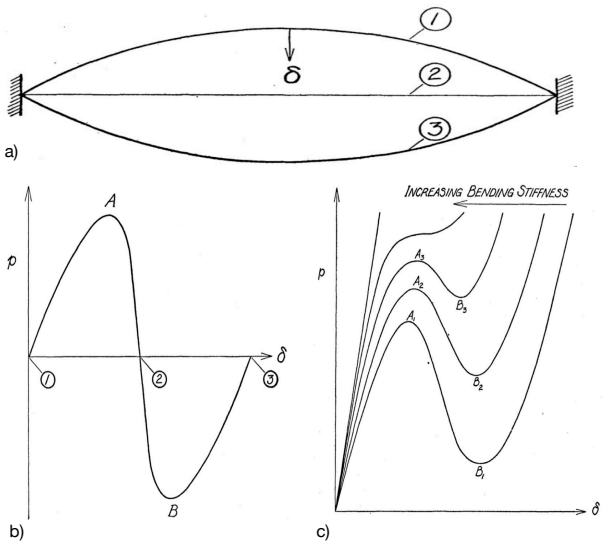

Fig. 1.1 A spherical membrane (a) subjected to a displacement δ is bistable (b) and the energy barrier between the states depends on the shell thickness (c) [21].

For the spherical membrane, the everted and original state have the same geometry and therefore the same stored strain energy. As the thickness is increased the barrier between the original and the everted state and the stored strain energy in the everted state increases. Brodland and Cohen studied the snap back of shallow spherical shells and showed that when

membrane forces are large enough to overcome bending forces the everted state is stable and the shell is bistable[3]. Brodland and Cohen used the shell half angle or half the solid angle of the cap, β, and a parameter combining the thickness and shell geometry, Λ. The parameters β and the geometric lengths, h and r, are shown in Fig. 1.2. Shallow shells in this context are defined as $\beta \cong h/r$. Λ is defined as:

$$\Lambda \cong (2h/t)\sqrt{12(1-\nu^2)}. \tag{1.13}$$

Since $h = r(1-cos\beta)$, Λ is also:

$$\Lambda \cong (2h/t)\sqrt{12(1-\nu^2)} = \frac{2r(1-cos\beta)}{t}\sqrt{12(1-\nu^2)}. \tag{1.14}$$

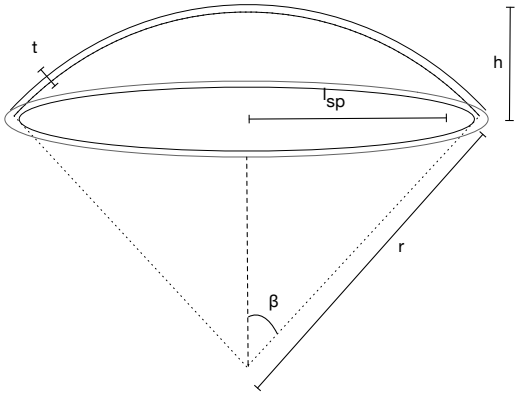

Fig. 1.2 Geometry of a spherical cap.

For large values of Λ^2, membrane forces dominate and the shell can be everted into another stable state. It is easy to be convinced of this fact as the extreme case is where the shell has no thickness and the everted state and the original state have the same geometry and are energetically equivalent. As Λ^2 is reduced bending forces begin to play a role in the observed deformation. For $\Lambda^2 < 100$, nonaxisymmetric deformations are observed[4]. Madhukar et. al use the same geometry dome (they define dome geometry by h and l) and

measure a critical thickness, t_c, for which they observe a transition between bistability and monostability[10]. Empirically they report for shallow domes where $0.15 < h/l_{sp} < 0.65$ that the critical thickness is given by:

$$\frac{t_c}{l_{sp}} = -0.0211 + 0.2203\frac{h}{l_{sp}} \tag{1.15}$$

with a root mean squared value of 0.9993 from a 11 point data set. It is interesting to note that this empirical relation implies that Λ^2 in addition to further knowledge of the dome geometry is required to determine the stability of the cap. Rather a simple cut off for Λ^2 is not sufficient to quantify the result of bending and membrane forces on the stability of the cap. I used the data Madhukar et. al plot in their figure reporting this critical thickness to find that Λ^2 varied from 450 to 5000 for the caps they tested[10]. When I look at their criterion Eq. 1.15, I notice that the intercept -0.0211 is less than 1% of the reported slope. Additionally, Madhukar et. al do not mention how they chose the 11 points used to obtain this fit. Fitting Madhukar et. al's values for the monostable domes with a fixed intercept through the origin, I obtain $\frac{t_c}{l_{sp}} = 0.2518\frac{h}{l_{sp}}$ with a poor r-squared value of 0.275. My interpretation is that there is not a sharp transition between monostability and bistability and that it is observed over a range of lambda values around 24(obtained using $\frac{t_c}{l_{sp}} = 0.2518\frac{h}{l_{sp}}$), 27(obtained using $\frac{t_c}{l_{sp}} \cong 0.2203\frac{h}{l_{sp}}$), with materials properties, the solid angle, boundary effects influencing this range.

More recently, Vella et. al examined the static stability of deep spherical shells using experiments, simulations and theoretical examination of deep spherical shells [19]. For deep shells(this parameter reduces to Λ for small β), they show with theory, experiment and simulations that for different values of Λ_d, given by Eq. 1.16, the shell displays different stability.

$$\Lambda_d = (12(1-\nu^2))^{1/4}\sqrt{\frac{r}{t}}\beta \tag{1.16}$$

The shell is 1) monostable where $\Lambda_d \lessapprox 5.75$, 2) snaps axisymmetrically for $5.75 \lessapprox \Lambda_d \lessapprox 7.2$, 3) snaps hysteretically for $7.2 \lessapprox \Lambda_d \lessapprox 7.7$, and 4) asymmetrically buckles for $7.7 \lessapprox \Lambda_d$.

1.2.3 Stability of conical shells

Real conical shells do not form perfect points at the tips. In fact the more accurate limiting cases of indentation of a real, non-idealized conical shells are: 1) plate deformation of a conical shell at its tip [22], 2) point indentation of a round tipped conical shell, 3) indentation of a flat topped conical shell[25], and 4) folding the inward edge of a conical frustum. Like spherical shells, conical frustum show bistability under certain conditions [25], and can be deformed to form a circular fold which may break into polygonal folds [9]. For a critical

load of

$$C = \frac{P}{2\pi E t^2 cos^2 \beta} = 1(3(1-\nu^2))^(1/2) \tag{1.17}$$

a diamond shaped buckling pattern like the one shown in Fig. 1.3 is observed.

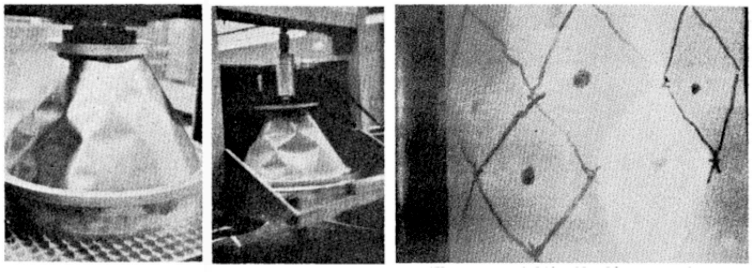

Fig. 1.3 Diamond shell buckling observed in a conical shell [22]

Bistability

Conical frustums are also known to show bistablility. The tip of a cone adds more complexity to understanding the behavior of conical shells. Recent studies have explored the stability of bendy straws, which are composed of multiple conical frustums attached as shown in Fig. 1.4 from [25]. Zhang's simulations show that individual pinned, conical frustums show bistable behavior for the conical angles and lengths common in bendy straw frustums [25]. Shallow, bistable conical shells are used in conical dielectric linear actuators [1] [5], and in the body to actuate eye movements [23].

1.2.4 Stability and boundary conditions

End conditions influence the stress strain response of the shell at a distance approximately that of $\sqrt{rt}$, or the square root of the radius of the shell times the thickness [21]. Using both a Finite Element (FE) Model and quadratically varying curvature (QVC) model, Seffen and Sobota show that allowing for some radial stiffness at the boundaries promotes bistability and when rotation is allowed at the boundary the shell responds in a non-uniform manner[18].

1.3 Pogorelov ridge in a spherical shell

Pogorelov described the geometry of a poked spherical shell, by considering that the shell will prefer to adopt isometric geometries, so the deformed shell can be considered as connected by 3 different regions: 1) an undeformed region, 2) a mirror buckled region where the shell is inverted, and 3) a ridge connecting these [14].

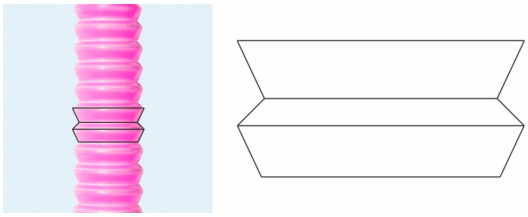

Fig. 1.4 The geometry of the bendy straws studied in Zhang's thesis on bistable conical shells [25]

Recently it has been discovered that actually the structure of a mirror buckled spherical shell consists of 7 different regions with different behavior [6]. Gomez and Vella solved the non-dimensional equations describing thin ($t << r$) spherical shells that deform axisymmetrically and without torsion in response to indentation to show that $\Delta = \frac{\delta}{t}$ is the relevant control parameter for the observed modes of the shell [6]. Eq.s 1.18 and 1.19 describe the behavior of thin ($t << r$) spherical shells that deform axisymmetrically and without torsion in response to indentation.

In equations Eq.1.18 and Eq. 1.19 ρ is the radial coordinate and ψ is the derivative of the Airy stress function satisfying Eq.1.20 and Eq.1.21.

$$D_B \nabla^4 w + \frac{1}{r}\frac{1}{\rho}\frac{d}{d\rho}(\rho\psi) - \frac{1}{\rho}\frac{d}{d\rho}(\psi\frac{dw}{d\rho}) = -\frac{F}{2\pi}\frac{\delta(\rho)}{\rho} \tag{1.18}$$

$$\frac{1}{Et}\rho\frac{d}{d\rho}(\frac{1}{\rho}\frac{d}{d\rho}\rho\psi) = \frac{\rho}{r}\frac{dw}{d\rho} - \frac{1}{2}(\frac{dw}{d\rho})^2 \tag{1.19}$$

$$\sigma_{\theta\theta} = \psi' \tag{1.20}$$

$$\sigma_{\rho\rho} = \frac{\psi}{\rho} \tag{1.21}$$

The non-dimensionallised variables shown in Eq. 1.22 through Eq. 1.25, rewrites the radial coordinate in terms of fractions of the geometric mean, the deflection in terms of fractions of the thickness, the Airy's stress in terms of the stretching stiffness multiplied by a geometric term, and the indentation load as it relates to the bending stiffness.

$$\bar{\rho} = \frac{\rho}{\sqrt{rt}} \tag{1.22}$$

$$\bar{w} = \frac{w}{t} \tag{1.23}$$

$$\bar{\psi} = \frac{\psi}{Et^2}\sqrt{\frac{r}{t}} \tag{1.24}$$

$$\bar{F} = \frac{Fr}{Et^3} \tag{1.25}$$

The non-dimensional forms of Eq. 1.18 and Eq. 1.19 obtained by using the non-dimensional forms Eq. 1.22 through Eq. 1.25 are shown in Eq. 1.26 and 1.27.

$$\frac{1}{12(1-\nu^2)}\nabla^4\bar{w}+\frac{1}{\bar{\rho}}\frac{1}{\rho}\frac{d}{d\bar{\rho}}(\bar{\rho}\,\bar{\psi})-\frac{1}{\bar{\rho}}\frac{d}{d\bar{\rho}}(\bar{\psi}\frac{d\bar{w}}{d\bar{\rho}})=-\frac{\bar{F}}{2\pi}\frac{\delta(\bar{\rho})}{\bar{\rho}} \tag{1.26}$$

$$\bar{\rho}\frac{d}{d\bar{\rho}}[\frac{1}{\bar{\rho}}\frac{d}{d\bar{\rho}}(\bar{\rho}\,\bar{\psi})]=\bar{\rho}\frac{d\bar{w}}{d\bar{\rho}}-\frac{1}{2}(\frac{d\bar{w}}{d\bar{\rho}})^2 \tag{1.27}$$

These non-dimensionalised equations, Eq. 1.26 and Eq. 1.27 are solved using the following boundary conditions.

$$\bar{w}(0)=-\Delta=\frac{\delta}{t} \tag{1.28}$$

$$\bar{w}'(0)=0 \tag{1.29}$$

$$\lim_{\rho\to\infty}(\bar{\rho}\,\bar{\psi}'(\bar{\rho})-\nu\,\bar{\psi}(\bar{\rho}))=0 \tag{1.30}$$

$$\bar{w}(\infty)=\bar{w}'(\infty)=\bar{\psi}(\infty)=0 \tag{1.31}$$

1.3.1 Factors influencing polygonal faceted ridges in spherical shells

The Pogorelov ridge is known to break into faceted, polygonal ridges for larger indentations in spherical shells amongst other shell geometries [20]. The underlying cause for the origin of the instability is unknown. Knoche and Kierfield suggest that a Euler buckling like mechanism underlies the polygonal fold formation. Gomez and Vella's analysis show that in one of the 7 identified regions in the deformed shell a compressive stress is present [6] [8]. Nasto and Reis explored the effect of an extensive number of factors on the character of the observed faceting: 1) indenter geometry, 2) indenter/shell frictional effects, and 3) non linear materials properties. Nasto and Reis used Neo-Hookean and linear elastic models. While Neo-Hookean and linear elastic materials behave differently, since the maximal strains in the deformed shells are up to 6%, the materials definition poses minimal influence on the observed effect. Since typical linear elastic materials(i.e. metals) plastically fail at strains of 1 to 2%, the observed polygonal folds are more commonly observed in shells made of hyperelastic materials [13], which can sustain strains of 6% without plastically failing. Nasto and Reiss quantify indenter effects by the ratio of the spherical indenter's radius to the radius of the shell, $\gamma=\frac{r_i}{r}$. They observe that for $\gamma\approx 1$, the formation of s-cones and gullies is frustrated and a largely uniform dimple is retained [13] [12]. For $\gamma<1$, they observe the polygonal faceted folds, while for $\gamma>2$ a qualitatively different behavior is observed.

Chapter 2

Experiments on Silicone Conical Shells

2.1 Initial observation of silicone conical shells

As mentioned in the introduction, the pliant silicone, conical shells (Back to Basics product number SIT10833) shown in Fig. 2.1 can be readily deformed to adopt a number of states in which the shell remains static while withstanding large deformations. When left sitting, the deformed shell showed no apparent changes even when left unloaded for extended periods of time(after a month no change was observed). Many of these deformed states are characterized by n-fold symmetry and localization of strain as seen in Fig. 2.1.

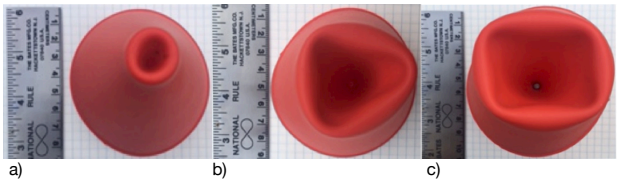

Fig. 2.1 The load free, poked conical shells deform to form "stable" circular folds (a) and polygonal folds (b and c).

2.2 Experimental set-up

2.2.1 Measurement of variation in conical shell thickness

2.2.2 Indentation and hysteresis measurements

A Tinius Olsen, Hounsfield 5 kN mechanical test machine was used in conjunction with a 5N load cell for the indentations less than 5mm, while the 250N was used for loadings where

larger deformations were applied to the shell. The force transducer used in the 5N load cell was calibrated according to the ISO700-1 or ASTM E 4 standard. Fig. 2.2 schematizes the experimental set-up. The load cell was used in displacement control. The load was applied at a rate of 5mm a second. To ensure observation of the inverted tip instead of axial buckling, a fold was initiated in the shell prior to loading. The tip was indented inwards. Then a steel rod (0.2kg) was pushed through a hole made in the tip and glued in place. To prevent the rod from moving, a cork was fixed to the inner end of the steel rod and securely hot glued in place. The geometry of the Back to Basics product number SIT10833 silicone conical shells is shown in Fig. 2.3; these shells have a cone angle 25°, are 12cm tall, and 1 to 2mm thick.

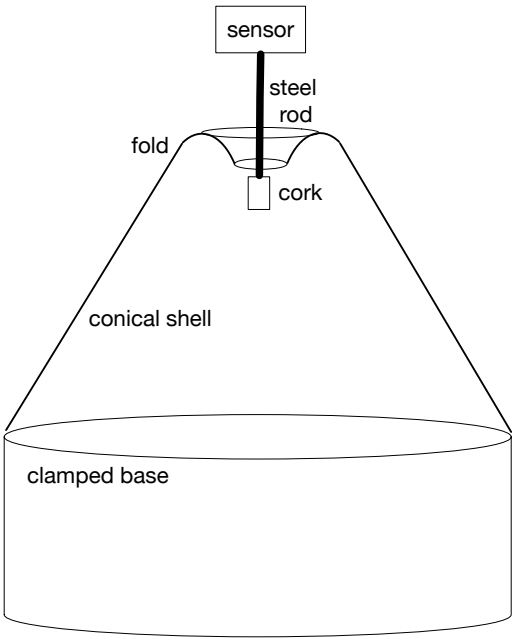

Fig. 2.2 Set-up used to apply loads δ_{start}, δ_{down}, and δ_{lift}

The shells were indented multiple times with the initial height of the initiated fold at a height of δ_{start}. Compression cycles were also performed where the shells were indented from a starting indenter depth of δ_{start} by a depth of δ_{down} and the position of the indenter was then retracted by a depth of δ_{lift} . These loading cycles are illustrated in Fig. 2.4.

I indented one conical shell 12 times by a $\delta_{down} = 140mm$ with a $\delta_{start} = 20mm$ at different speeds shown in Table 2.1. On the same conical shell I carried out hysteresis measurements. Table 2.2 shows the hysteresis measurements carried out on the same cone. I did find it difficult to observe the same fold formation reproducibly using a reproducible method with these shells, even though manually I could stimulate the folded deformation with a pen or by folding the outer edge with my hands.

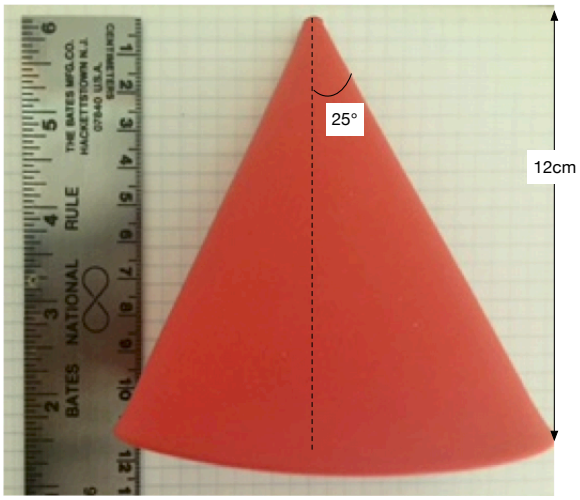

Fig. 2.3 The geoemetry of tested silicone conical shells.

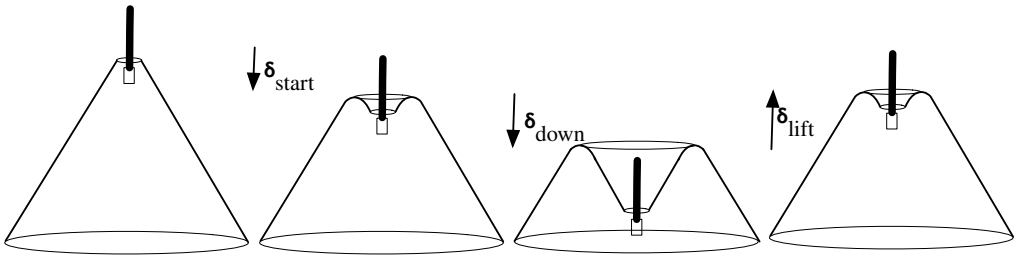

Fig. 2.4 A fold was initiated in the shell by by a distance δ_{start} followed by applications of δ_{down} and δ_{lift} respectively.

Table 2.1 Indentation experiment loading conditions

Test	δ_{start}(mm)	δ_{down}(mm)	δ_{lift}(mm)	speed (mm/s)
Indentation 26	20	140	0	10
Indentation 27	20	140	0	10
Indentation 28	20	140	0	10
Indentation 29	20	140	0	15
Indentation 30	20	140	0	15
Indentation 31	20	140	0	20
Indentation 32	20	140	0	25
Indentation 33	20	140	0	30
Indentation 34	20	140	0	20
Indentation 35	20	140	0	20
Indentation 36	20	140	0	35
Indentation 37	20	140	0	40

Table 2.2 Hysteresis experiment loading conditions

Test	δ_{start}(mm)	δ_{down}(mm)	δ_{lift}(mm)
Cycle 1	20	2	2
Cycle 2	20	2	2
Cycle 3	20	2	2
Cycle 4	20	10	10
Cycle 5	20	10	10
Cycle 6	20	10	10
Cycle 7	20	10	10
Cycle 8	20	10	10
Cycle 9	20	10	10
Cycle 10	20	40	40
Cycle 11	20	40	40
Cycle 12	20	40	40
Cycle 13	20	40	40
Cycle 14	20	40	40
Cycle 15	20	100	100
Cycle 16	20	100	100
Cycle 17	20	35	35
Cycle 18	20	35	35
Cycle 19	20	30	30
Cycle 20	20	30	30
Cycle 21	20	25	25
Cycle 22	20	25	25
Cycle 23	20	22	22
Cycle 24	20	22	22
Cycle 25	20	20	20
Cycle 26	20	20	20
Cycle 27	20	15	15
Cycle 28	20	15	15
Cycle 29	20	12	12
Indent 30	20	15	0
Cycle 31	20+15	20	20
Cycle 32	20+15	15	15

2.3 Results

2.3.1 Non-uniformity in shells

As a result of slight variations in each of the silicone conical shells and slight variations in initial conditions, slight variations in the observed shell response may be observed. Table 2.3 reports measured variations in the thickness of shells obtained from 3 different conical shells obtained from this same company.

Table 2.3 Variation observed in conical shells

Sample		Mean	Std. Dev	Var
	Top	1.15	0.0868	0.00753
A	Middle	1.14	0.0713	0.00509
	Base	1.22	0.0595	0.00354
	All	1.17	0.0792	0.00627
	Top	1.14	0.210	0.0443
B	Middle	1.13	0.147	0.0217
	Base	1.18	0.143	0.0204
	All	1.15	0.164	0.0276
	Top	1.1	0.102	0.0105
C	Middle	1.01	0.0460	0.00211
	Base	1.04	0.0486	0.00236
	All	1.05	0.0812	0.00660
	Top	1.13	0.141	0.0199
All	Middle	1.09	0.113	0.0128
	Base	1.15	0.116	0.0135
	All	1.12	0.125	0.0156

2.3.2 Indentation of different shells

2.3.3 Hysteresis

I performed 28 different compression cycles where I loaded the shell as depicted in Fig. 2.4. The conditions for each of these cycles is given in Table 2.2. One of each of the repeats of a given compression cycles is plotted in Fig. 2.6.

Table 2.4 shows the hysteresis between all similar cycles. While the hysteresis between initial cycles and cycles where the indenter did not travel distances comparable to the size of the fold is significant, hysteresis between some of the cycles is small (<.32%) and of the same order as hysteresis reported by pneumatic actuators used in industry [2]. While these

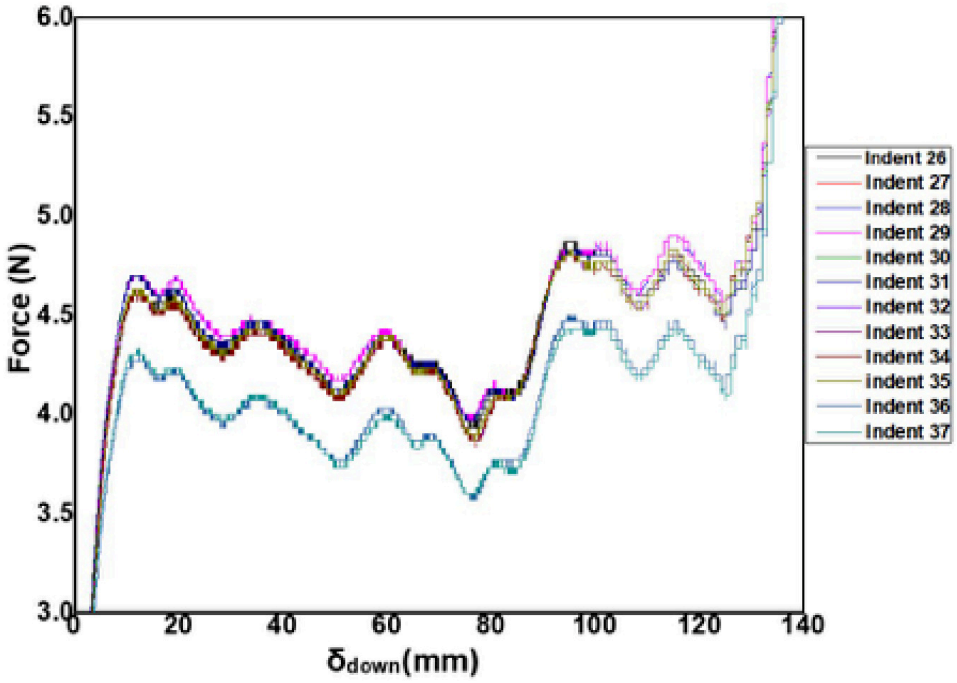

Fig. 2.5 Twelve different indentations of the same shell carried out at different speeds.

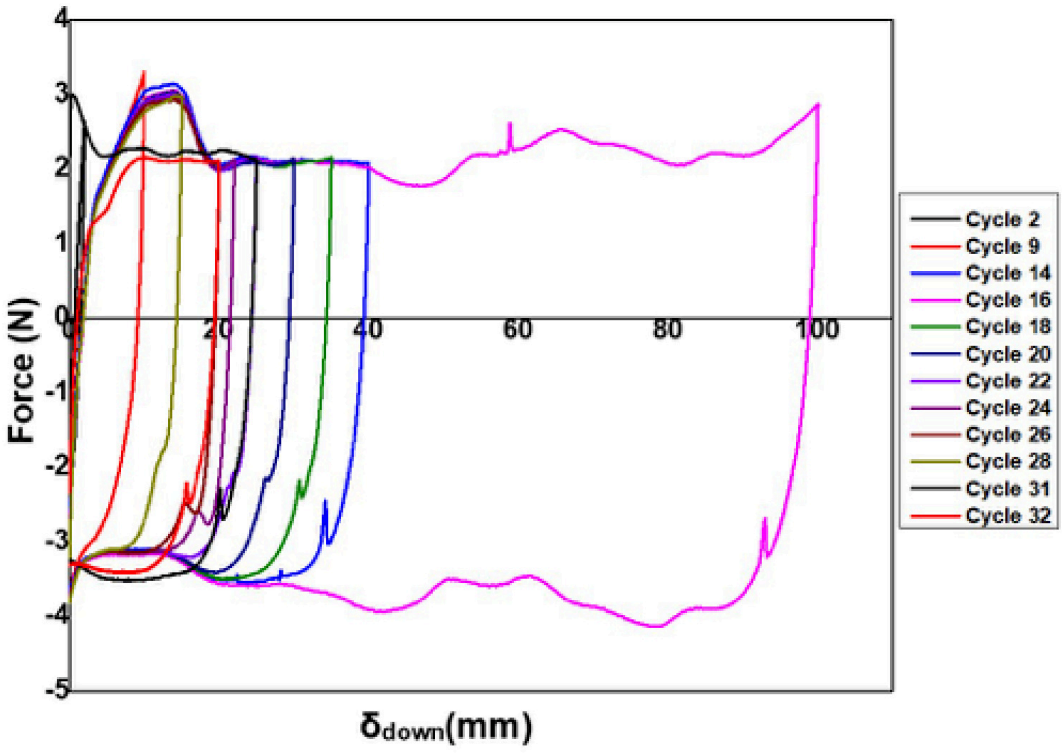

Fig. 2.6 Shell response to different indentation depths and unloading

measurements are not extensive enough to fully assess the behavior of this object, these results are noteworthy and interesting to investigate as they suggest that at least in these limited samples for some loadings a relatively elastic deformation is being observed. Why and what the dissipative process is accounting for the observed hysteresis is unclear.

Table 2.4 Hysteresis between cycles

δ_{start}(mm)	Cycle pair	Hysteresis %
2	Cycle 1 and 2	37.0
2	Cycle 2 and 3	6.00
10	Cycle 4 and 5	21.1
10	Cycle 5 and 6	2.16
10	Cycle 6 and 7	0.690
10	Cycle 7 and 8	1.03
10	Cycle 8 and 9	0.547
40	Cycle 10 and 11	1.81
40	Cycle 11 and 12	1.18
40	Cycle 12 and 13	0.340
40	Cycle 13 and 14	0.0197
100	Cycle 15 and 16	1.24
35	Cycle 17 and 18	0.520
30	Cycle 19 and 20	0.295
25	Cycle 21 and 22	0.258
22	Cycle 23 and 24	0.630
20	Cycle 25 and 26	0.463
15	Cycle 27 and 28	1.21

Hysteresis

A peak was observed as the indenter was lifted in Cycles 10, 11, 12, 13, 14, 15, 16, 17, 18, 19, 20, 21, 22, 23, 24, 25, 26, 31 and 32. For cycles 31 and 32, the δ_{start} was 15mm lower than for the other loading sequences.The peaks from one of each loading are plotted as a function of δ_{lift} in Fig. 2.7.

A slight lateral load was also applied to the shell in Cycle 11 by jostling the cone; the response of the shell to the slight lateral is 0.1N, which is much smaller than the peak observed in Fig. 2.7.

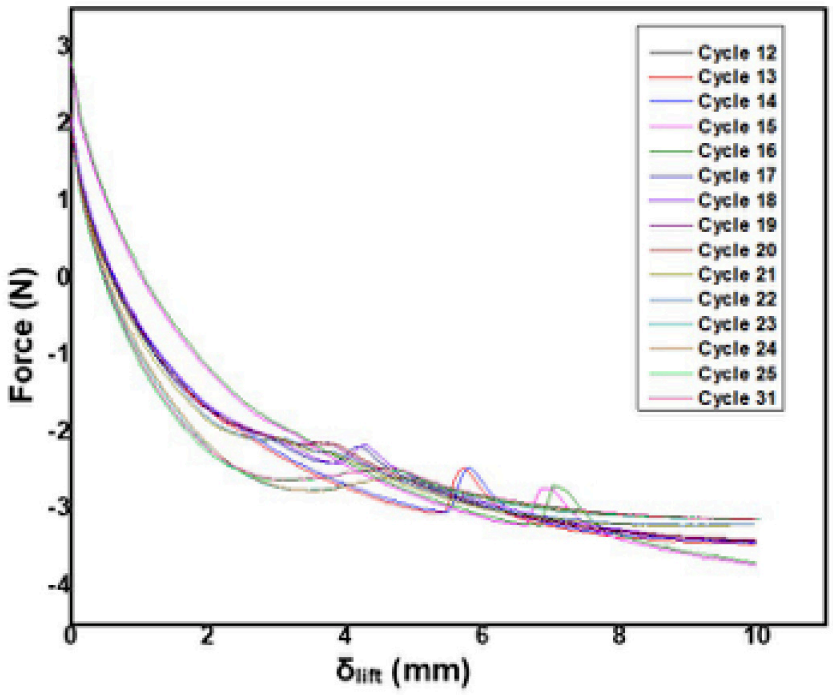

Fig. 2.7 Where the shell was indented by a distance larger than 20mm, a peak was observed in the shell response as the load was removed for a δ_{lift} between 3 and 9mm.

2.4 Discussion

One hypothesis for explaining the observed peak is that energy is stored in the released fold. The peak is not due to just random noise. It does appear that the deformation processes after an initial loading sequence are largely elastic as hysteresis between later cycles is on the order of a few percent. I note that the number of samples quantitatively studied are not sufficient to prove that this behavior is indeed elastic. It would have been more ideal to have had a number of samples and a number of tests. One problem to address in testing a larger number of samples is a more robust method of quantifying variation in the shells than a simple caliper measure of the thickness of the shell. Observation of the inverted fold requires a well centered sample and an indenter that is small compared to the tip. Shells with a more pronounced and large spherical tip (more like the geometries simulated in the next geometry) will likely make an interesting and simpler system to further study.

Chapter 3

FEM Simulation of Indented Spherically Capped Conical Shells

3.1 Shell geometry: spherically capped conical shells

To initiate the deformation where a fold is formed in a conical shell, I chose to model the indentation of a smoothly joined spherical cap and conical frustum.

3.1.1 Constraints imposed on a tangential spherical cap by a fully parametrised conical frustum

For a conical frustum of slant height l, cone angle α, and the radius of the shell's base R, the number of tangent spherical caps that can be placed on the frustum are constrained in spherical radius r, and solid angle β as shown in Fig. 3.1.

In order for the spherical cap to be tangent with the conical shell the cone angle and the half angle of the spherical cap are related as follows.

$$\beta = \pi/2 - \alpha \tag{3.1}$$

The green and yellow triangles in Fig. 3.1 highlight the relationship between β and α. All the triangles shaded in Fig. 3.1 (the yellow, green, and blue) are similar. The hypotenuse of the yellow triangle is the same length as the radius of the spherical cap, r. The side of the yellow triangle opposite the angle β has a length of $rsin\beta = rsin(\pi/2 - \alpha) = rcos\alpha$. The radius of the shell's base, R, and the spherical shell radius, r, are related by Eq. 3.2.

$$rcos\alpha = R - lsin\alpha \tag{3.2}$$

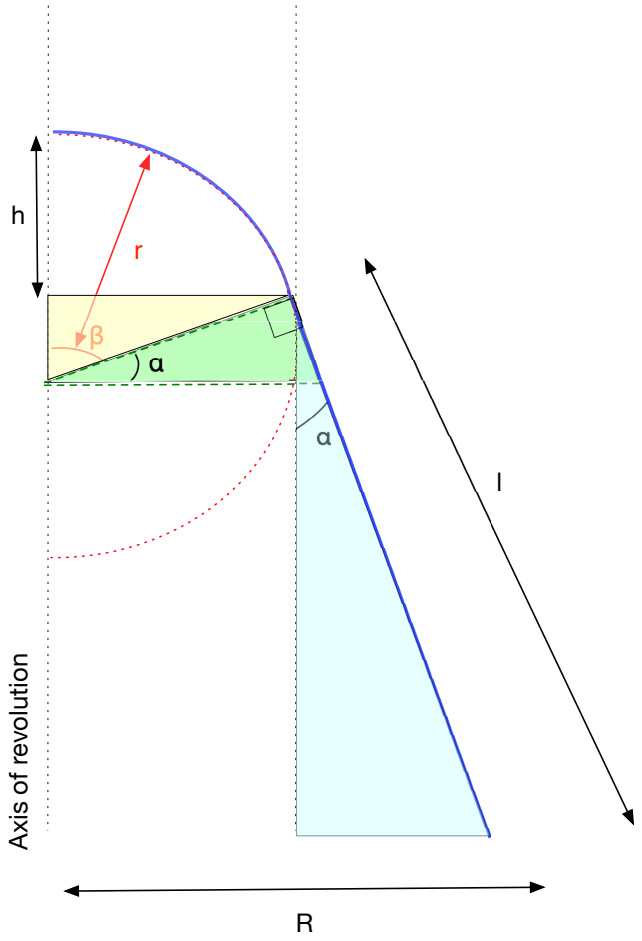

Fig. 3.1 Relevant geometric lengths describing a spherically capped conical shell.

Since both the solid angle, 2β, and the spherical cap radius, r are constrained when forcing a spherical cap to be tangent to a conical frustum with shell base radius, R, cone angle, α, and frustum slant height l, there is only one radius, r, and solid angle sector, 2β, of a spherical surface which can be fit onto a defined conical frustum. As r approaches $lsin\alpha$, the geometry of the surface approaches a pure conical surface that comes to a point at the tip. The geometry of a spherically capped conical frustum surface where the cap and frustum are tangent is fully defined by 3 parameters R, l, and α. For a shell of the same surface geometry a 4th parameter, the thickness t, is required to fully define the geometry of the shell. As shown in Fig. 3.2, as α is varied from 0 to $\pi/2$, the surface varies from a flat circular plate of radius l to a hemispherical cap attached to a cylinder of length l. In between these extremum, the surface is a spherical cap of solid angle $\beta = \pi/2 - \alpha$ attached to a conical shell of steepness α and slant height l. As the base radius of the shell, R, is varied from $R = lsin\alpha$, to $R >> l$ the surface varies from a pointed, perfectly conical surface to a spherical cap with a small conical rim.

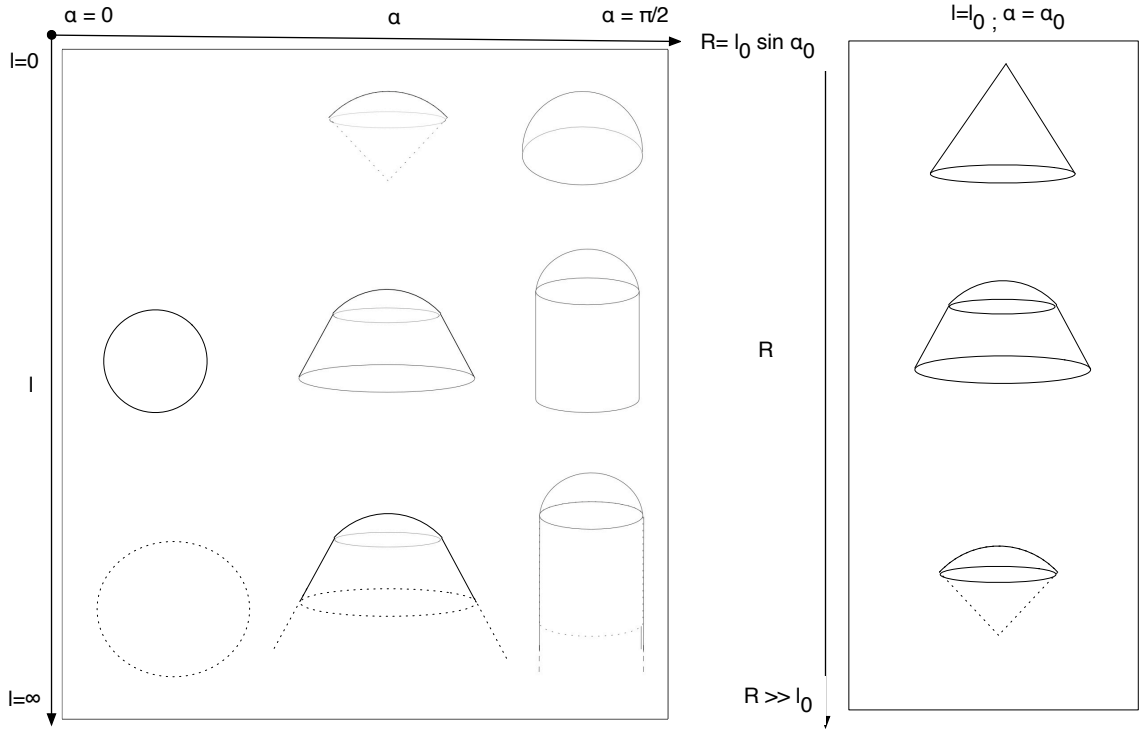

Fig. 3.2 Variation of cap and conical geometry as a function of the minimal parameters describing this surface, α, l, and R

As stated in the introduction for spherical caps the transition between monostability and bistability depends on the cap height, h, which is related to the cap radius, r, and α by

$$h = r(1 - sin(\alpha)). \tag{3.3}$$

3.2 Finite Element Method (FEM) methods

I used ABAQUS /CAE (SIMULIA, Providence, RI)'s FEM software package to simulate the indentations of spherical capped conical shells and load conical frustums with a bending moment. The indentations of the spherically capped conical shells were carried out under quasi-static conditions. The default Standard Explicit Solver was used.

3.2.1 Boundary conditions and meshing

For all simulations (both the indentations of the spherically capped conical shells and the bending moment loaded conical frustums)the shell base was clamped to force no rotations and no displacements at the shell base edge. Hemispherical analytically rigid spherical shells with radii of r_i were used to indent the spherically capped conical shells. These indenters were subjected to a displacement control boundary condition. S3R and S4 elements were used for all shells. While the seeds used to generate the mesh were evenly spaced the meshes were not perfectly symmetric.

3.2.2 Materials definitions

A hyperelastic, Neo-Hookean material with Neo-Hookean coefficients of $C_{10} = 227300Pa$ and $D_1 = 2.36x10^{-8}Pa^{-1}$ was used for the shell model. For one simulation a linear elastic material definition with E=1MPa was used instead for the shell model. The stress-strain curves for the materials definitions is shown in Fig. 3.3. Since I used a Poisson ratio of $\nu = 0.49$, the simulations largely treat the shell as though it is made of an incompressible material.

When zoomed in near $\lambda = 1$ which corresponds to low strains, the hyperelastic curve is very close to linear Fig. 3.4. However, the Young's modulus I chose is less stiff than the hyperelastic material for this strain region.

3.2.3 FEM parameter summary

All parameters for all simulations are summarised in Table 3.1. In the results, only those plots needed to show the general trend are shown.

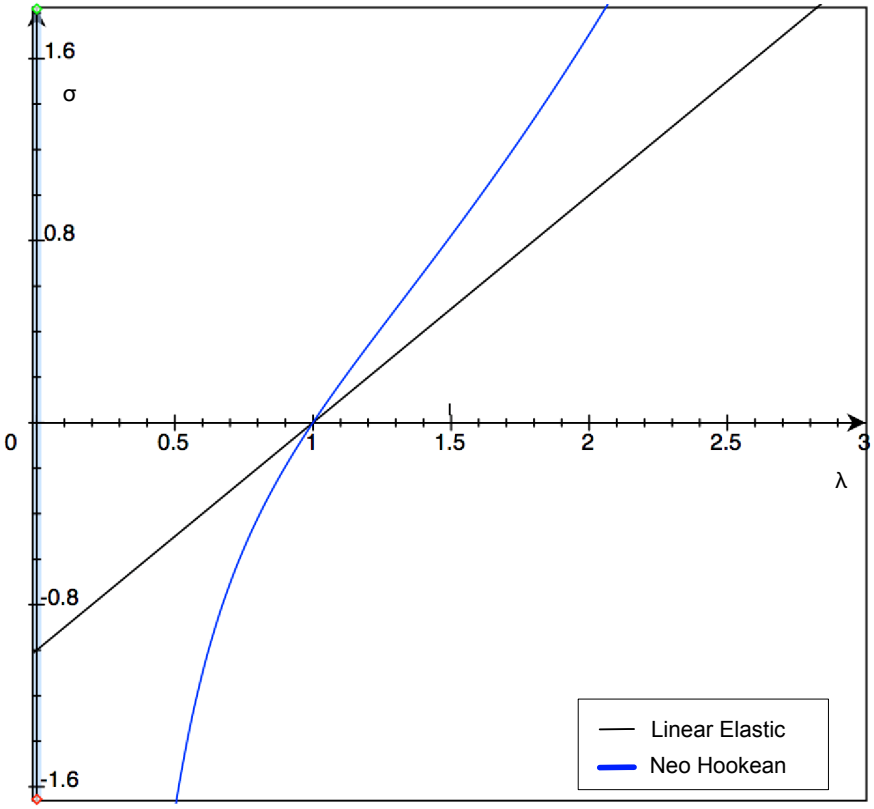

Fig. 3.3 Neo-Hookean and linear elastic materials definitions used in this thesis.

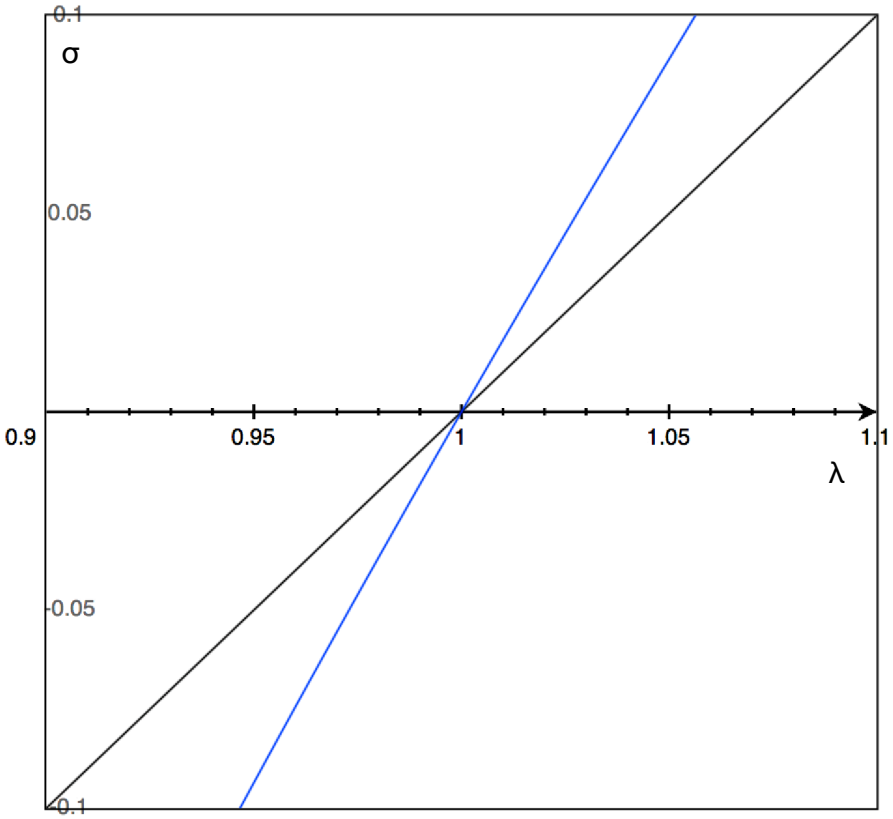

Fig. 3.4 Neo-Hookean and linear elastic materials definitions used in this thesis.

Table 3.1 Summary of FEM parameters

curve name	r (mm)	h(mm)	α (rad)	l (mm)	t(mm)	r_i	material	Λ_d
25deg31	20	11.2	0.436	20	0.31	0.5	hyperelastic	15.8
25deg32	20	11.2	0.436	20	0.32	0.5	hyperelastic	15.5
25deg35	20	11.2	0.436	20	0.35	0.5	hyperelastic	14.9
25deg37sl	20	11.2	0.436	15	0.37	0.5	hyperelastic	14.5
25deg37	20	11.2	0.436	20	0.37	0.5	hyperelastic	14.5
25deg37	20	11.2	0.436	20	0.37	0.5	linear elastic	14.5
25deg37sl30	20	11.2	0.436	30	0.37	0.5	hyperelastic	14.5
25deg37sl35	20	11.2	0.436	35	0.37	0.5	hyperelastic	14.5
25deg37sl40	20	11.2	0.436	40	0.37	0.5	hyperelastic	14.5
25deg37sl45	20	11.2	0.436	45	0.37	0.5	hyperelastic	14.5
25deg37r15	20	11.2	0.436	20	0.37	0.15	hyperelastic	14.5
25deg37r25	20	11.2	0.436	20	0.37	0.25	hyperelastic	14.5
25deg37r6	20	11.2	0.436	20	0.37	0.6	hyperelastic	14.5
25deg37r7	20	11.2	0.436	20	0.37	0.7	hyperelastic	14.5
25deg37r8	20	11.2	0.436	20	0.37	0.8	hyperelastic	14.5
25deg40	20	11.2	0.436	20	0.40	0.5	hyperelastic	13.9
25deg43	20	11.2	0.436	20	0.43	0.5	hyperelastic	13.4
25deg47	20	11.2	0.436	20	0.47	0.5	hyperelastic	12.8
25deg53	20	11.2	0.436	20	0.53	0.5	hyperelastic	12.1
25deg58	20	11.2	0.436	20	0.58	0.5	hyperelastic	11.5
25deg65	20	11.2	0.436	20	0.65	0.5	hyperelastic	10.9
25deg67	20	11.2	0.436	20	0.67	0.5	hyperelastic	10.7
25deg75	20	11.2	0.436	20	0.75	0.5	hyperelastic	10.1
25deg77	20	11.2	0.436	20	0.77	0.5	hyperelastic	10.0
25deg82	20	11.2	0.436	20	0.82	0.5	hyperelastic	9.71
30deg30	20	9.53	0.524	20	0.3	0.5	hyperelastic	14.8
30deg35	20	9.53	0.524	20	0.35	0.5	hyperelastic	13.7
30deg40	20	9.53	0.524	20	0.4	0.5	hyperelastic	12.8
30deg45	20	9.53	0.524	20	0.45	0.5	hyperelastic	12.1
30deg5	20	9.53	0.524	20	0.5	0.5	hyperelastic	11.5
35deg4	20	7.78	0.611	20	0.4	0.5	hyperelastic	11.8
35deg45	20	7.78	0.611	20	0.45	0.5	hyperelastic	11.1
35deg5	20	7.78	0.611	20	0.5	0.5	hyperelastic	10.5
45deg	20	4.29	0.785	20	0.45	0.5	hyperelastic	9.07
25degsn1	3.31	1.91	0.436	11.6	0.04	conc	hyperelastic	17.9
25degsn2	3.31	1.91	0.436	11.6	0.05	conc	hyperelastic	16.0
35degsn1	7.32	3.12	0.611	7.41	0.04	conc	hyperelastic	22.5
35degsn2	7.32	3.12	0.611	7.41	0.05	conc	hyperelastic	20.1
35degsn3	7.32	3.12	0.611	7.41	0.06	conc	hyperelastic	18.4
35degsn4	3.66	1.56	0.611	7.41	0.04	conc	hyperelastic	15.9
35degsn5	3.66	1.56	0.611	7.41	0.05	conc	hyperelastic	14.2
35degsn6	3.66	1.56	0.611	7.41	0.06	conc	hyperelastic	13.0

3.3 Results

I found it difficult to obtain initial inversion for thick shells with similar size geometry as snow cone(25degsn1, 25degsn2, 35degsn1, 35degsn2, 35degsn3, 35degsn4, 35degsn5, 35degsn6). None of the simulations of a similar geometry could be converged beyond the initial penetration of the dimple into the spherical cap region. However, when I introduced a large cap on the conical rims, I was able to simulate penetration of the polygonal folds into the conical region. When plotting all of the indentations the following features are observed: 1) a change in slope for a given $\frac{\delta}{t}$(this is a well established and explained response of the spherical cap) which is associated with observation of a polygonal ridge, 2) a buckling threshold after which the shell does not resist much, 3) sometimes preceded by a former peak, and 4) a stiffening of the shell as indentation proceeds well past the cap/cone join. Of these four features, the last 3 are not governed by the control parameter $\frac{\delta}{t}$.

3.3.1 Spherically capped conical shell buckling threshhold

I plotted the shell response for the parameter $\delta_j = \frac{\delta}{h}$ as shown in Fig.3.5 . The buckling is observed for $\delta_j = \frac{\delta}{h}$ varying between 1.67 and 2.25.

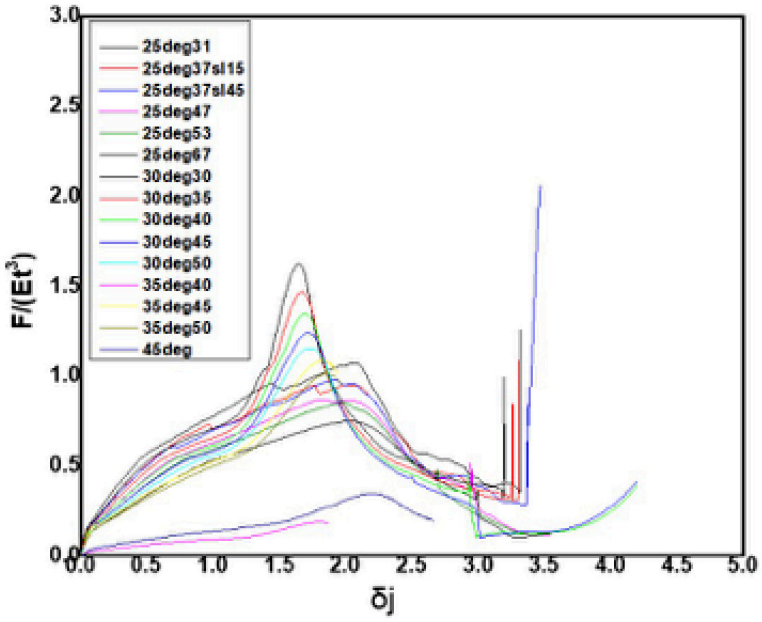

Fig. 3.5 Buckling of the shells is observed for $\delta_j = \frac{\delta}{h}$ varying between 1.67 and 2.25

For the 17 simulations where $\alpha = 25\ ^\circ = 0.436$ rad shells of varying thickness, indenter type, slant height with the same cap of $r = 20mm$, $h = 11.2mm$, the transition is observed at $\delta_j \approx 2$. For the 4 simulations $\alpha = 30\ ^\circ = 0.524$ rad shells of varying thickness, indenter type, slant height with the same cap of $r = 20mm$, $h = 9.53mm$, the transition is observed at $\delta_j \approx 1.67$. For the 3 simulations $\alpha = 35\ ^\circ = 0.611$ rad shells of varying thickness, indenter type, slant height with the same cap of $r = 20mm$, $h = 7.78mm$, the transition is observed at $\delta_j \approx 1.75$. The only simulation of a shell with $\alpha = 45\ ^\circ = 0.785$ rad ,$r = 20mm$, and $h = 4.29mm$ $\delta_j \approx 2.25$. These values are summarised in Table 3.2. These transition values are almost perfect rational fractions(i.e 1.67 = 5/3, 1.75 = 7/4, 2 = 2/1, and 2.25 = 9/4).

Table 3.2 Observed δ_j for different α shell with $r = 20mm$

α(deg/rad)	δ_j
25°(0.436 rad)	2
30°(0.524 rad)	1.67
35°(0.611 rad)	1.75
45°(0.785 rad)	2.25

3.3.2 Ridge radius and shell response

I plotted the shell response for the parameter $\delta_{ridge} = \frac{\delta}{\sqrt{r\delta}}$ as shown in Fig.3.6 . Buckling of the shells is observed for δ_{ridge} between 0.667 and 1.1.

For the 17 simulations where $\alpha = 25\ ^\circ = 0.436$ rad shells of varying thickness, indenter type, slant height with the same cap of $r = 20mm$, $h = 11.2mm$, the transition is observed at $\delta_{ridge} \approx 1$.

For the 4 simulations $\alpha = 30\ ^\circ = 0.524$ rad shells of varying thickness, indenter type, slant height with the same cap of $r = 20mm$, $h = 9.53mm$, the transition is observed at $\delta_{ridge} \approx 0.9$.

For the 3 simulations $\alpha = 35\ ^\circ = 0.611$ rad shells of varying thickness, indenter type, slant height with the same cap of $r = 20mm$, $h = 7.78mm$, the transition is observed at $\delta_{ridge} \approx 0.84$.

The only simulation of a shell with $\alpha = 45\ ^\circ = 0.785$ rad, $r = 20mm$, and $h = 4.29mm$ $\delta_{ridge} \approx 0.67$. These values are summarised in Table 3.3.

3.3.3 Extending the conical rim

Fig. 3.7 shows the stiffness of simulations where $\alpha = 25\ ^\circ = 0.436$ rad, $r = 20mm$, $h = 11.2mm$, and $t = 0.37mm$ wheres the slant height differs. The overall shape of the responses of each of these shells remains the same including the buckling of the shell. Buckling of the

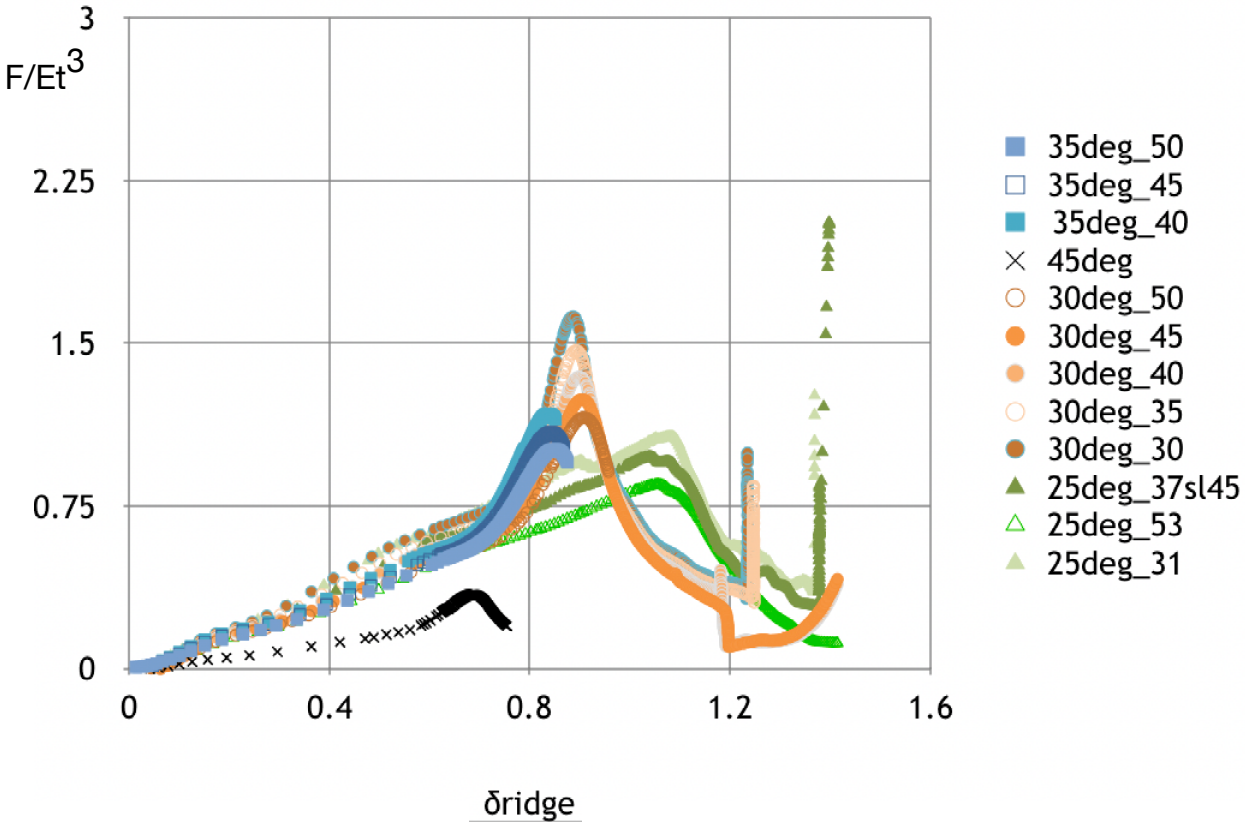

Fig. 3.6 Softening of shells observed for $\delta_{ridge} = \frac{\delta}{\sqrt{r\delta}}$ varying between 0.6 and 1.1

Table 3.3 Observed δ_{ridge} for different α shell with $r = 20mm$

α(deg/rad)	δ_{ridge}
25deg (0.436 rad)	1
30deg (0.524 rad)	0.9
35deg (0.611 rad)	0.84
45deg (0.785 rad)	0.67

shell is preceded by a jump in the stiffness, which occurs after the split of three ridges into four.

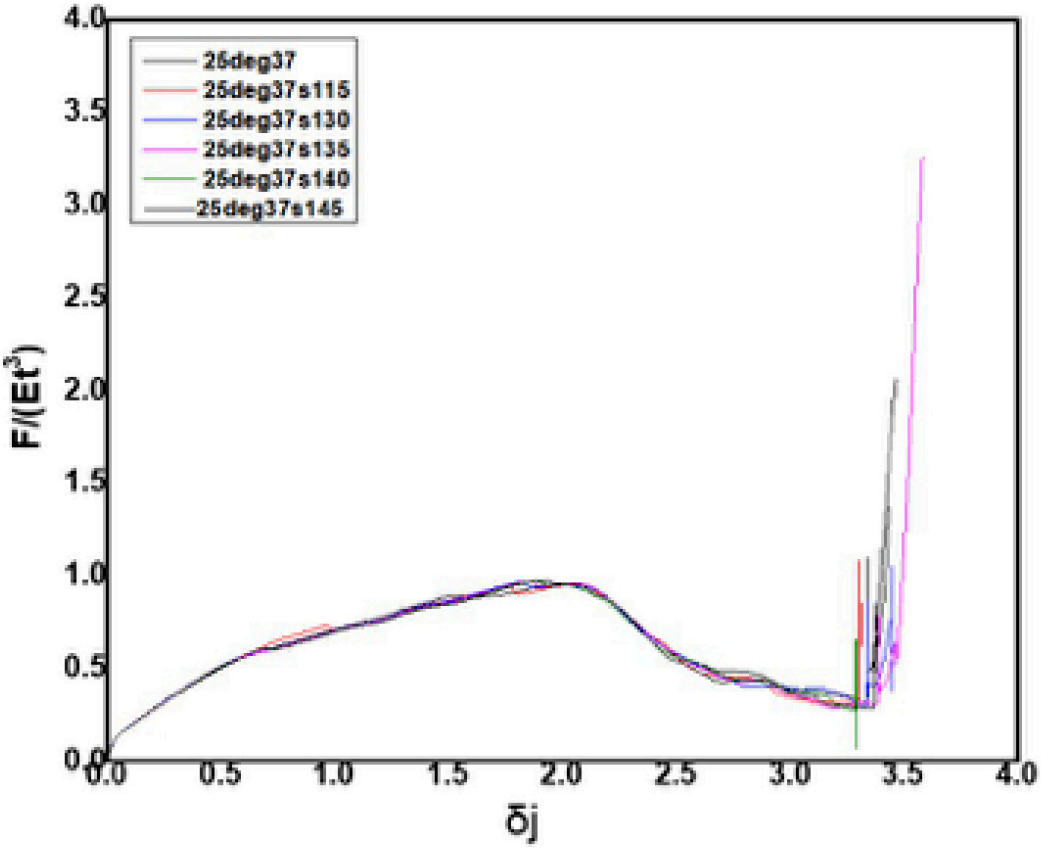

Fig. 3.7 Extending the conical shell slant height does not change the overall response but some of the hysteretic jumps shift.

3.3.4 Observed modes

Polygonal fold formation is initiated while the fold is still in the spherical cap region for all simulations. 7.7 $\lessapprox \Lambda_d$, so asymmetric buckling is expected and consistent with previous studies on spherical caps. The formation of a 4 faceted polygonal fold happens as the deformed ridge is nearing the join between the spherical cap and the conical frustum. A hysteretic jump and sudden softening of the shell are observed for the same δ as the 4 faceted polygonal fold.

3.4 Discussion: Spherical and conical shell join

Since the primary novel feature observed in this work, a buckling of the shell, which is sometimes preceded by a peak is not predicted by Δ, this feature is not purely explained by descriptions of shallow indentations of a spherical shell. A possible explanation for the observed response, is that this response is due to a combination of the spherical and conical shell geometry. If this is the case, it is reasonable to expect that major changes in the stiffness response of the shell are likely to be observed as the ridge is in the region where the cap and shell are tangent.

3.4.1 Parameter δ_j

If a perfect crease formed as the spherically capped conical shell was indented, this crease would reach the join between the cap and shell for a $\delta_j = 2$. Therefore the fact that the observed transition occurs for a δ_j between 1.67 and 2.25 is in agreement with this explanation. It is also interesting that these transition values are almost perfect rational fractions(i.e 1.67 = 5/3, 1.75 = 7/4, 2 = 2/1, and 2.25 = 9/4)

Since r and h are related by Eq. 3.3, δ_j is also given by Eq. 3.4, which reveals why this transition is dependent on the conical angle α.

$$\delta_j = \frac{\delta}{h} = \frac{\delta}{r(1-sin\alpha)} \tag{3.4}$$

Another way of thinking about this is that the tangent between the cone and the cap forces the cap to be of a certain solid angle. It is interesting that the shell responses for $\alpha = 25\,\text{deg}$, show this feature for δ_j exactly at 2.

3.4.2 Parameter δ_{ridge}

Another way to conceptualise the cap and conical geometry, is to consider the ridge radius of an axisymmetric ridge. In a spherical shell this ridge radius is given by $r_{ridge} = \sqrt{r\delta}$. It is interesting that the shell responses for $\alpha = 25\,^{\circ}$, show this feature for δ_j exactly at 2, and for this same data set the transition is observed at $\delta_{ridge} = 1$. It is interesting to note that all other α data sets do not show the pronounced hysteretic jump observed in the $\alpha = 25\,^{\circ}$prior to this softening. Both δ_{ridge} and δ_j are related as shown in Eq. 3.5. This relationship might lead you to expect that $\delta_{capcone}$ is the parameter capturing the behaviour of a spherically capped conical shell. Table3.4 reflects that while the transition for all of the data sets is around $\delta_{capcone} \approx 1$, there is some variation in $\delta_{capcone}$.

$$\delta_{capcone} = (1 - sin\alpha)\frac{\delta_j}{\delta_{ridge}} = \sqrt{\frac{\delta}{r}} \tag{3.5}$$

Table 3.4 Observed $\delta_{capcone}$ for different α shell with $r = 20mm$

α(deg/rad)	$(1 - sin\alpha)\frac{\delta_j}{\delta_{ridge}}$
25°(0.436 rad)	1.15
30°(0.524 rad)	0.93
35°(0.611 rad)	0.89
45°(0.785 rad)	0.98

3.4.3 Extending the conical shell

As extending the slant height, l, creates a self similar conical shell with the same thickness, I would have expected that if any of the response of the shell was a result of the conical geometry, a lowering in stiffness would be observed. The only change in shell response is in the hysteretic jump observed before the sudden softening, and for the most part, qualitatively the shell response does not change even when the slant height is tripled. The geometry of the join between the spherical cap and the conical shell dominates the behavior of the shell for the range of r, l, and α simulated. For different theories of deformations of a flat plate the behavior of the plate changes with ratio of the plate length to thickness, so in a similar vein I would like to know what are the regimes governing this particular shell response.

3.4.4 Polygonal Folds

All of the geometries of the spherical caps used have $7.7 \lessapprox \Lambda_d$, so asymmetric buckling is expected. The formation of four polygonal folds is observed in all of the simulations as the fold nears the join between the spherical cap and the conical frustum.

3.4.5 The behavior of the join between the spherical cap and the conical frustum

The FEM work raises some specific questions, which I am presenting as a list.

- Does $\delta_{capcone}$ capture the behavior of a different cap radius, spherically capped conical shell?

- For the α simulated, the transition was observed at δ_j that appear to be ratios of whole numbers(1.67 = 5/3, 1.75 = 7/4, 2 = 2/1, and 2.25 = 9/4). Is this a coincidence? If not why?
- For $\alpha = 25deg$, the buckling was observed for $\delta_j = 2$ and $\delta_{ridge} = 1$ suggesting that the softening occurred when the radius was that for a Pogorelov ridge in a spherical cap of the same radius for δ corresponding to that which would be observed in a shell with a perfect crease
  - What is the geometry of the ridge at this transition in these shells compared to those with other values of α.
  - Is the structure of the fold like that in a spherical shell?
  - Is there any connection between this and formation of a 4 faceted fold structure happened to occur during this transition?

Chapter 4

Conclusions

4.1 Summary of main findings

- The silicone snow shell provided an everyday example of an object which stimulated the question about how geometry and materials resulted in observed load free, deformed shells
- Attaching a spherical cap to a conical frustum provided a method for initiating a fold in the conical shell and studying the behavior of this more complex shell
- The behavior of the spherically capped conical shell showed a buckling event related to the join between the spherical cap and the conical shell
- Simulations of indentations of a spherically capped conical shells showed a buckling transition for large δ where the $\delta_{buckling}$ is common to the same α shell
  - This feature was observed for shells of varying α, varying t, varying l, and the same cap radius for a $\delta_{capcone} \approx 1$
  - Sometimes this feature was preceded by a hysteretic jump
  - Formation of a 4 faceted fold structure happened to occur during this transition

4.2 Conclusions

4.2.1 Unusual stability of the silicone conical shells

The snow cone provided a number of interesting phenomena as a starting place for this thesis. I observed that when I deformed the shell either by poking the tip or by folding an edge,

that the shell adopted a folded state that remained stable without any load for over a month. The fold in the shell was either perfectly circular or broke into polygonal folds. The shell smoothly transitioned between a fold at almost any height where the tip was inverted to a fold a few centimeters away from the edge. I observed that the shell could sit load free for even up to a month (perhaps longer) in this deformed state. The experiments did show that for the sample tested over multiple cycles after the initial few, there was small hysteresis between loadings suggesting that in this case, the deformation of the shell is probably largely elastic in nature. While many shells show bistability, or even some kind of multistability, I have not found reports of many manmade objects with this almost analog- like static stability. By analog-like stability, I mean a stability that appears to be over an infinite number of large, finite, continuous displacements of the shell's coordinates. In contrast, spherical caps have two stable states that are not slight perturbations of each other. Biological muscles like the tongue are able to adopt a number of states like the folded conical shell, but this is due to an input of energy from the biological system, and not the same kind of static stability observed in the silicone conical shells. Plain conical frustum again show bistability, but not the complicated stability of multiple states observed in these conical shells.

While the FEM simulations of the spherically capped conical shells do not show the same analog like stability, multiple buckling events are also observed in the responses of the spherically capped conical shells to indentation.

4.2.2 Method to study stability of the observed stability

Experimentally, I found that indentation allowed me to more quantitatively study and more clearly describe the behaviour of the silicone shells. Idealising the shape of the shell as a spherical cap connected to a conical frustum allowed me to simplify the geometric parameters describing the shells. This idealisation gave the basis for using FEM to study the indentation of a spherically capped conical shell.

4.2.3 Join between the spherical cap and the cone

Since the cap and conical frustum are smoothly joined, fixing the radius and extent of the spherical cap also fixes the angle of the conical frustum. For each set of simulations of conical shells of the same angle and same size cap, a buckling event is observed for the same value of $\delta_{capcone}$. For the shells studied, extending the extent of the conical shell or changing l does not change the $\delta_{capcone}$ at which the buckling event was observed. Also varying the thickness does not change the observed buckling events. This is interesting as changing the thickness changes the bending stiffness of the shell. It is also striking that even when the

conical shell is extended, the geometry of the join between the spherical cap and the conical shell still dominates the shell response.

4.2.4 Polygonal folds

In the silicone conical shells, the tips of the shells are not perfectly spherical. Polygonal buckling is observed in the shells and a buckling event is observed when the shell transitions from three polygonal folds to four polygonal folds. In the silicone conical shells the polygonal fold formation is clearly initiated while the fold is in a clearly conical geometry of the shell. In the FEM simulations of spherically capped conical shells, asymmetric buckling is initiated before the fold is clearly in the conical region of the shell, however a splitting of one of the 3 polygonal folds into 4 polygonal folds is observed as the fold nears the join between the spherical cap and the conical frustum.

4.3 Further work

The behavior observed in the silicone conical shells is likely largely due to the material properties of the silicone shell. Local imperfections in the studied conical shells made it difficult to obtain reproducible and reliable results. A full characterisation of the shell material, the full shell geometry(including local imperfections) along with visualisation of the deformed shell would provide more information on the influence of geometry and material on the observed stability. Full characterisation of the local geometry of the silicone conical shells might suggest other FEM experiments as well. Investigation of a silicone conical shell with a large spherical tip like the FEM results presented in the third chapter would give further insight into interplay between material properties and geometry and the actual observed stability.

References

[1] Berselli, G., Vertechy, R., Vassura, G., and Castelli, V. P. (2017). Effects of boundary conditions on bistable behaviour in axisymmetrical shallow shells. *Proceedings of the Royal Society A*, 473(2203):1–20.

[2] BrayCommercial (2017). Industrial pneumatic actuators series 92 / 93 - features and benefits bi-directional travel stops industrial actuators. "Brochure". [online] https:// braycommercialdivision.com/.

[3] Brodland, G. and Cohen, H. (1987). Deflection and snapping of spherical caps. *International Journal of Solids and Structures*, 23(10):1341–1356.

[4] Bushnell, D. (1967). Bifurcation phenomena in spherical shells under concentrated and ring loads. *American Instititute of Aeronautics and Astronautics*, 5(11):2034–2040.

[5] Dubowsky, S., Hafez, M., and Lichter, M. (2008). Dielectric elastomer actuated systems and methods. US Patent 7,411,331.

[6] Gomez, M., Moulton, D. E., and Vella, D. (2016). The shallow shell approach to pogorelov's problem and the breakdown of 'mirror buckling '. *Proceedings of the Royal Society A: Mathematical, Physical and Engineering Sciences*, 472(2187):20150732.

[7] Guest, S. and Pellegrino, S. (2006). Analytical model for bistable cylindrical shells. *Proceedings of the Royal Society A*, 462:839–854.

[8] Knoche, S. and Kierfeld, J. (2014). The secondary buckling transition: Wrinkling of buckled spherical shells. *The European Physical Journal*, 37:62.

[9] Lobkovsky, A. E. (1996). *Structure of Crumpled Thin Elastic Membranes*. PhD thesis, University of Chicago.

[10] Madhukar, A., Perlitz, D., Grigola, M., Gai, D., and Hsia, K. J. (2014). Bistable characteristics of thick-walled axisymmetric domes. *International Journal of Solids and Structures*, 51(14):2590–2597.

[11] Mott, P. H., Dorgan, J., and Roland, C. (2008). The bulk modulus and poisson's ratio of 'incompressible' materials. *Journal of Sound and Vibration*, 312:572– 575.

[12] Nasto, A., Ajdari, A., Lazarus, A., Vaziri, A., and Reis, P. M. (2013). Localization of deformation in thin shells under indentation. *Soft Matter*, 9:6796.

[13] Nasto, A. M. (2011). Localization of deformation in thin shells under indentation. Master's thesis, Massachusetts Institute of Technology.

[14] Pogorelov, A. V. and Babenko, V. I. (1992). Geometric methods in the theory of stability of thin shells. *Prikl. Mekhanika*, 28(28):3–21.

[15] Pritz, T. (2007). The poisson's loss factor of solid viscoelastic materials. *Journal of Sound and Vibration*, 306:790– 802.

[16] Santer, M. (2010). Self-actuated snap back of viscoelastic pulsing structures. *International Journal of Solids and Structures*, 47(24):263–3271.

[17] Shahzad, M., Kamran, A., Siddiqui, M. Z., and Farhan, M. (2015). Mechanical characterization and fe modeling of a hyperelastic material. *Materials Research*, 18:918–924.

[18] Sobota, P. M. and Seffen, K. A. (2017). Effects of boundary conditions on bistable behaviour in axisymmetrical shallow shells. *Proceedings of the Royal Society A: Mathematical, Physical and Engineering Sciences*, 473(2203):20170230.

[19] Taffetani, M., Jiang, X., Holmes, D. P., and Vella, D. (2018). Static bistability of spherical caps. *Proceedings of the Royal Society A: Mathematical, Physical and Engineering Sciences*, 474(2213):20170910.

[20] Vaziri, A. and Mahadevan, L. (2008). Localized and extended deformations of elastic shells. *Proceedings of the National Academy of Sciences*, 105(23):7913–7918.

[21] Von Karman, T. and Tsien, H. (1939). The buckling of spherical shells by external pressure. *International Journal of Solids and Structures*, 7(2):43–50.

[22] Weingarten, V. I., Morgan, E. J., and Seide, P. (1964). Elastic stability of thin- walled cylindrical and conical shells under axial compression. *American Institute of Aeronautics and Astronautics*, 3:500– 505.

[23] Woon, W. H., Greig, D., Savage, M. D., Wilson, M. C. T., Grant, C. A., Bishop, F., and Mokete, B. (2015). Asymmetric vitreomacular traction and symmetrical full thickness macular hole formation. *Graefe's Archive for Clinical and Experimental Ophthalmology*, 253:1851–1857.

[24] Yang, W., Li, Z.-M., Shi, W., Xie, B.-H., and Yang, M.-B. (2004). Review: On auxetic materials. *Journal of Materials Science*, 39:3269–3279.

[25] Zhang, B. (2016). *Bistable and Multi-stable Thin Walled Structures*. PhD thesis, University of Oxford, Department of Engineering Science.